Institute of
Applied Mechanics
Institut für Baumechanik

Graz University of Technology

Preprint Series

Institute of Applied Mechanics

Graz University of Technology

Preprint No 03/2010

A Regularized Collocation Boundary Element Method for Linear Poroelasticity

Michael Messner, Martin Schanz
Institute of Applied Mechanics, Graz University of Technology

Accepted for publication in: *Computational Mechanics*
Latest revision: December 16, 2010

Abstract

This article presents a collocation boundary element method for linear poroelasticity, based on the first boundary integral equation with only weakly singular kernels. This is possible due to a regularization of the strongly singular double layer operator, based on integration by parts, which has been applied to poroelastodynamics for the first time.

For the time discretization the convolution quadrature method (CQM) is used, which only requires the Laplace transform of the fundamental solution. Furthermore, since linear poroelasticity couples a linear elastic with an acoustic material, the spatial regularization procedure applied here is adopted from linear elasticity and is performed in Laplace domain due to the before mentioned CQM. Finally, the spatial discretization is done via a collocation scheme.

At the end, some numerical results are shown to validate the presented method with respect to different temporal and spatial discretizations.

1 Introduction

As for boundary element formulations in general, their development is strongly linked to the availability of fundamental solutions. In the field of poroelasticity, Manolis and Beskos [17] first used a set of Laplace domain governing equations based on Biot's theory, for which they derived a fundamental solution. Therewith, these authors developed a Laplace domain boundary element method, leading to time domain results via numerical inversion schemes. Neglecting friction between the two constituents of a poroelastic material, Wiebe and Antes [29] were able to transform the just mentioned Laplace domain fundamental solution in a closed form back to time domain, allowing them to establish a direct time domain BEM for their reduced model. The next step was done by Schanz [24], who moved on by using the convolution quadrature method (CQM) developed by Lubich [15, 16], allowing him to realize a direct time domain formulation for the complete model just requiring the Laplace transform fundamental solution. As pointed out in [24], the latter method has some advantages over inverse transformations, e.g., no restrictions concerning transient boundary conditions. More details on boundary element methods in linear poroelasticity can be found in [7, 25].

These previous observations were related to the temporal aspect of linear poroelasticity when working with boundary integral equations (BIE). However, dealing with the spatial aspect always causes some trouble, too. This is due to the singular behavior of the fundamental solution within the integral operators. Hence, one has to distinguish whether only the first or also the second BIE is involved. In the engineering community a common approach is to use collocation schemes for the discretization of the first boundary integral equation. Such methods are justified by their simplicity and computational efficiency compared to other schemes such as Galerkin methods. There, to exploit the advantageous symmetry of the method [11], the second boundary integral equation needs to be included. The latter equation involves a boundary integral operator with a hypersingular kernel function (hypersingular operator). Nevertheless, the restriction to the first boundary integral equation still requires the evaluation of the double layer operator. This is a boundary integral operator with strongly singular kernel, whose evaluation is not straightforward within a numerical scheme. Due to the strong relation between poroelasticity and linear elasticity on one side and acoustics on the other side, a look at these fields is given to get an idea how to cope with this difficulty.

Apart from analytical integration, which is limited to some distinct element types and, therefore, not desired within a general scheme, there exist two main approaches to deal with this matter. On one hand, there are numerical approaches as introduced by Martin and Rizzo [19] for two dimensional wave scattering or by Guiggiani and Gigante [8] which allows the evaluation of Cauchy singular boundary integrals arising from three dimensional analysis. The latter technique has already been applied to linear poroelasticity by Schanz [24], however, it involves adding and subtracting the singular part of the fundamental solution's asymptotic behavior. In this case, one has to subtract the frequency independent elastostatic fundamental solution from the frequency dependent poroelastodynamic fundamental solution. This may cause numerical instability because at higher frequencies the frequency dependent part dominates. Furthermore, the implementation differs between collocation and Galerkin type approaches, which is not favorable for an extension to the latter methods. On the other hand, there are analytical regularization techniques based on integration by parts, dealing with the kernel as a whole, thus they do not

show the above discussed problem of numerical instability. Such an approach was first applied by Maue [20] to scalar wave scattering and by Kupradze [14] to linear elasticity in the field of potential theory. Almost at the same time Nedelec [22] proposed a regularization for acoustics as well as for linear isotropic elastic problems, an extension of which to the anisotropic case can be found in [2]. Nishimura and Kobayashi [23] presented similar results but with respect to a collocation scheme, giving some remarks comparing the two approaches. As all previously mentioned regularization techniques for the linear elastic system involving integration by parts, the approach by Han [10], which is based on the original work of Kupradze [14], is also concerned with the hypersingular operator. However, as a side product it yields a regularization of the double layer operator. In the here presented approach, this result is adapted to poroelasticity, resulting in a weakly singular first boundary integro-differential equation in Laplace domain. This is another advantage of this approach – within a numerical scheme the same treatment of all operators is possible, since all of them show the same regularity.

The procedure throughout this article is as follows: In section 2, Biot's theory is recalled in a suitable manner for the later development of the boundary element formulation in section 3. As pointed out by Lubich [15], advantage is taken of the CQM being especially suitable for the discretization of time convolutions, where only the Laplace transformed kernel is known a priori. Moreover, due to the use of the reformulated version by Banjai and Sauter [1], the time domain problem is decoupled into a set of Laplace domain problems. Thus, the boundary integral equation is derived in subsection 3.1 and regularized in subsection 3.2, both in Laplace domain. Then, in subsection 3.3 the time discretization of the formal time domain BIE is done via CQM, before in subsection 3.4 for the spatial discretization a collocation scheme is used. In section 4, two numerical examples are presented: First, the proposed method is verified by comparing it with a semi-analytic solution, whereas the second example's aim is to show one of the boundary element methods' strength, i.e., the capability of dealing with (semi-)infinite domains such as a half-space.

Some remarks on the notation: Bold lower case letters are used for vectors and bold upper case letters for matrices in the context of the fundamental solution. Tensors are denoted by lower case Greek symbols and the nabla operator acting with respect to the point $\mathbf{x} = [x_1, x_2, x_3]^\top$ is defined as $\nabla_{\mathbf{x}} := [\partial_{x_1}, \partial_{x_1}, \partial_{x_2}]^\top$. Laplace transformed quantities are identified by $\mathcal{L}[f(t)] := \hat{f}(s)$ with $s \in \mathbb{C}$ and time derivatives by $\partial_t f(t) := \dot{f}(t)$. Finally, all multiplications are to be understood in the sense of matrix multiplications.

2 Biot's Theory

Considering a linearized three-dimensional setting, Biot's theory [3, 4] leads to a set of second order partial differential equations describing the state of a saturated poroelastic continuum in some domain $\Omega \subset \mathbb{R}^3$.

According to Biot's theory, a poroelastic medium consists of a solid skeleton with volume V^s, intersected by some interconnected fluid filled pores with volume V^f. The fraction of the fluid volume over the total volume $V = V^f + V^s$ is defined as the porosity

$$\phi = \frac{V^f}{V} \,. \tag{1}$$

With Biot's effective stress coefficient $\alpha = \phi(1 + Q/R)$ the constitution of the total stress tensor σ is given by

$$\sigma = 2\mu\varepsilon + (\lambda \operatorname{tr}\varepsilon - \alpha p)\,\mathbf{I}\,, \tag{2}$$

where λ and μ are the Lamé parameters of the bulk material, and Q and R describe the coupling between the fluid and the solid phase. The pore pressure is denoted by p and the linear strain tensor ε is defined as

$$\varepsilon = \frac{1}{2}\left(\nabla\mathbf{u}^\top + (\nabla\mathbf{u}^\top)^\top\right) \tag{3}$$

relating the solid strain state with the solid displacement field $\mathbf{u}$. Furthermore, a kind of constitutive equation for the variation of the fluid volume per reference volume ζ is introduced as

$$\zeta = \alpha \operatorname{tr}\varepsilon + \frac{\phi^2}{R}p\,. \tag{4}$$

This variation of the fluid volume per reference volume has to obey the continuity equation

$$\dot{\zeta} + \nabla^\top\mathbf{q} = 0\,, \tag{5}$$

with the specific flux $\mathbf{q} = \phi(\dot{\mathbf{u}}^f - \dot{\mathbf{u}})$ where $\mathbf{u}^f$ is the fluid displacement field. The total stress, on the other hand, must fulfill the balance of momentum for the bulk material

$$\left(\nabla^\top\sigma\right)^\top + \mathbf{F} = \rho\ddot{\mathbf{u}} + \phi\rho^f(\ddot{\mathbf{u}}^f - \ddot{\mathbf{u}})\,, \tag{6}$$

with body forces $\mathbf{F}$, the bulk density ρ, and the fluid density ρ^f. A generalized form of Darcy's law [24] is used to describe the flux trough the pores

$$\mathbf{q} = -\kappa\left(\nabla p + \rho^f\ddot{\mathbf{u}} + \frac{\rho_a + \phi\rho^f}{\phi}(\ddot{\mathbf{u}}^f - \ddot{\mathbf{u}})\right)\,, \tag{7}$$

where κ denotes the dynamic permeability. The apparent mass density ρ_a was introduced by Biot himself and is defined as $\rho_a = C\phi\rho^f$. For the low frequency range $C = 0.66$, otherwise it is frequency dependent [6].

There are different possibilities to combine the above equations in order to obtain the equations of motion. However, as shown by Bonnet [5] it is sufficient to chose $\mathbf{u}$ and p to describe the poroelastic continuum in Laplace domain. Moreover, having the later use of the CQM in mind, this formulation is absolutely sufficient. Thus, assuming homogeneous initial conditions for the Laplace transformation of the above equations and combining them appropriately, a homogeneous mixed boundary value problem in linear poroelasticity in terms of the generalized displacement field $\hat{\mathbf{u}}^g = [\hat{\mathbf{u}}, \hat{p}]^\top$ is stated by

$$\begin{aligned}
\hat{\mathcal{B}}_{\tilde{\mathbf{x}}}\hat{\mathbf{u}}^g(\tilde{\mathbf{x}}) &= \mathbf{0} \quad \text{for} \quad \tilde{\mathbf{x}} \in \Omega\,,\\
\hat{\mathbf{u}}^g(\mathbf{x}) &= \hat{\mathbf{g}}_D \quad \text{for} \quad \mathbf{x} \in \Gamma_D\,,\\
\hat{\mathbf{t}}^g(\mathbf{x}) &= \hat{\mathbf{g}}_N \quad \text{for} \quad \mathbf{x} \in \Gamma_N\,.
\end{aligned} \tag{8}$$

The differential operator is defined as

$$\hat{\mathcal{B}}_{\tilde{\mathbf{x}}} = \begin{bmatrix} \mathcal{B}^e_{\tilde{\mathbf{x}}} + s^2(\rho - \beta\rho^f)\, I & (\alpha-\beta)\nabla_{\tilde{\mathbf{x}}} \\ s(\alpha-\beta)\nabla^\top_{\tilde{\mathbf{x}}} & -\frac{\beta}{s\rho^f}\Delta_{\tilde{\mathbf{x}}} + \frac{s\phi^2}{R} \end{bmatrix} \tag{9}$$

and the generalized tractions as

$$\hat{\mathbf{t}}^g(\mathbf{x}) = \begin{bmatrix} \mathcal{T}^e_{\mathbf{x}} & -\alpha\mathbf{n}_{\mathbf{x}} \\ s\beta\mathbf{n}^\top_{\mathbf{x}} & \frac{\beta}{s\rho^f}\mathbf{n}^\top_{\mathbf{x}}\nabla_{\mathbf{x}} \end{bmatrix} \begin{bmatrix} \hat{\mathbf{u}}(\mathbf{x}) \\ \hat{p}(\mathbf{x}) \end{bmatrix}, \tag{10}$$

with $\mathcal{B}^e_{\tilde{\mathbf{x}}}$ being the differential operator of linear elastostatics and $\mathcal{T}^e_{\mathbf{x}}$ its traction operator reflecting Hooke's law.

3 Boundary Element Formulation

3.1 Boundary Integral Equation

The representation formula related to the homogeneous problem (8) is given by

$$\hat{\mathbf{u}}^g(\tilde{\mathbf{x}}) = \left(\hat{\mathcal{V}}\hat{\mathbf{t}}^g\right)_\Omega(\tilde{\mathbf{x}}) - \left(\hat{\mathcal{K}}\hat{\mathbf{u}}^g\right)_\Omega(\tilde{\mathbf{x}}) \quad \text{for} \quad \tilde{\mathbf{x}} \in \Omega\,, \tag{11}$$

with the integral operators

$$\left(\hat{\mathcal{V}}\hat{\mathbf{t}}^g\right)_\Omega(\tilde{\mathbf{x}}) = \int_\Gamma \hat{\mathbf{U}}^\top(\mathbf{y}-\tilde{\mathbf{x}})\ \hat{\mathbf{t}}^g(\mathbf{y})\,\mathrm{d}s_{\mathbf{y}}\,, \tag{12}$$

$$\left(\hat{\mathcal{K}}\hat{\mathbf{u}}^g\right)_\Omega(\tilde{\mathbf{x}}) = \int_\Gamma \left(\hat{\mathcal{T}}_{\mathbf{y}}\hat{\mathbf{U}}\right)^\top(\mathbf{y}-\tilde{\mathbf{x}})\ \hat{\mathbf{u}}^g(\mathbf{y})\,\mathrm{d}s_{\mathbf{y}}\,. \tag{13}$$

In (12) and (13), $\hat{\mathbf{U}}$ is the complex conjugated fundamental solution of the adjoint problem and $\hat{\mathcal{T}}_{\mathbf{y}}$ the related traction operator, which naturally appears throughout the derivation of the representation formula. Skipping all arguments for sake of readability, they are defined as

$$\hat{\mathbf{U}} = \begin{bmatrix} \hat{\mathbf{U}}^s & \hat{\mathbf{U}}^f \\ \left(\hat{\mathbf{P}}^s\right)^\top & \hat{P}^f \end{bmatrix} \qquad \hat{\mathcal{T}}_{\mathbf{y}} = \begin{bmatrix} \mathcal{T}^e_{\mathbf{y}} & s\alpha\mathbf{n}_{\mathbf{y}} \\ -\beta\mathbf{n}^\top_{\mathbf{y}} & \frac{\beta}{s\rho^f}\mathbf{n}^\top_{\mathbf{y}}\nabla \end{bmatrix}, \tag{14}$$

where $\hat{\mathbf{U}}$ may be found in full detail in appendix A.1. The most important property within the context of this paper is the singular behavior of the individual parts in $\hat{\mathbf{U}}$ in combination with the properties of $\hat{\mathcal{T}}_{\mathbf{y}}$, which is subject of subsection 3.2.

Equation (11) describes the unknown field $\hat{\mathbf{u}}^g$ inside the domain for given Cauchy data, which are not known yet. For their computation, a limiting process $\Omega \ni \tilde{\mathbf{x}} \to \mathbf{x} \in \Gamma$ is performed, in which (12) is well defined and commonly referred to as single layer operator

$$\lim_{\Omega\ni\tilde{\mathbf{x}}\to\mathbf{x}\in\Gamma}\left(\hat{\mathcal{V}}\hat{\mathbf{t}}^g\right)_\Omega(\tilde{\mathbf{x}}) = \left(\hat{\mathcal{V}}\hat{\mathbf{t}}^g\right)(\mathbf{x}) := \int_\Gamma \hat{\mathbf{U}}^\top(\mathbf{y}-\mathbf{x})\ \hat{\mathbf{t}}^g(\mathbf{y})\,\mathrm{d}s_{\mathbf{y}}\,. \tag{15}$$

More important for the further understanding of this article, however, is the result of this limiting process performed on (13) due to the strong singularity of the kernel function in its classical form. Its derivation is standard technique, therefore only the final result is recalled here [28]

$$\lim_{\Omega \ni \tilde{\mathbf{x}} \to \mathbf{x} \in \Gamma} \left(\hat{\mathcal{K}} \hat{\mathbf{u}}^g \right)_\Omega (\tilde{\mathbf{x}}) = \left[-I(\mathbf{x}) + \mathcal{C}(\mathbf{x}) \right] \hat{\mathbf{u}}^g(\mathbf{x}) + \left(\hat{\mathcal{K}} \hat{\mathbf{u}}^g \right)(\mathbf{x}) \ , \tag{16}$$

where $I(\mathbf{x})$ is the identity operator, the jump term $\mathcal{C}(\mathbf{x})$ is defined as

$$\mathcal{C}(\mathbf{x}) := \lim_{\varepsilon \to 0} \int\limits_{\mathbf{y} \in \Omega : |\mathbf{y}-\mathbf{x}| = \varepsilon} \left(\hat{\mathcal{T}}_{\mathbf{y}} \hat{\mathbf{U}} \right)^\top (\mathbf{y}-\mathbf{x}) \, \mathrm{d}s_{\mathbf{y}} \tag{17}$$

and the double layer operator as

$$\left(\hat{\mathcal{K}} \hat{\mathbf{u}}^g \right)(\mathbf{x}) := \lim_{\varepsilon \to 0} \int\limits_{|\mathbf{y}-\mathbf{x}| \geq \varepsilon} \left(\hat{\mathcal{T}}_{\mathbf{y}} \hat{\mathbf{U}} \right)^\top (\mathbf{y}-\mathbf{x}) \ \hat{\mathbf{u}}^g(\mathbf{y}) \, \mathrm{d}s_{\mathbf{y}} \ . \tag{18}$$

Collecting these previous results, one ends up with the Laplace domain BIE

$$\mathcal{C}(\mathbf{x}) \hat{\mathbf{u}}^g(\mathbf{x}) = \left(\hat{\mathcal{V}} \hat{\mathbf{t}}^g \right)(\mathbf{x}) - \left(\hat{\mathcal{K}} \hat{\mathbf{u}}^g \right)(\mathbf{x}) \ . \tag{19}$$

Finally, with an inverse Laplace transformation the formal time domain BIE for a homogeneous poroelastodynamic problem with homogeneous initial conditions reads as

$$\mathcal{C}(\mathbf{x}) \mathbf{u}^g(\mathbf{x},t) = \left(\mathcal{V} * \mathbf{t}^g \right)(\mathbf{x},t) - \left(\mathcal{K} \mathbf{u}^g \right)(\mathbf{x},t) \ , \tag{20}$$

where the $*$ operator denotes the convolution in time

$$(f * g)(t) = \int_0^t f(t-\tau) \, g(\tau) \, \mathrm{d}\tau \quad \text{for} \quad t \in (0,T) \ . \tag{21}$$

Other than that all operators are defined analogously as in Laplace domain.

3.2 Regularization of the Double Layer Operator

As outlined in the title of this article, the aim is to work with kernels of certain regularity, i.e., showing at most weak singularities. Motivated by the arguments given in the introduction, the same regularization technique as in [11, 12], which itself is based on Han's work, is used. However, only the necessary ingredients for its understanding are recalled, whereas further details may be found in [11].

The idea is to integrate (13) by parts first, which leads to a kernel function with higher regularity, before the limiting process (16) is performed. As a consequence of this regularization, the extension of this operator to the boundary only involves the jump term of Laplace' equation. This finding is of special interest, since for the later presented collocation BEM formulation a point-wise evaluation of the BIE is required and due to this fact the evaluation of the jump term even at corner points remains rather simple.

The poroelastodynamic fundamental solution inherits the singularities from linear elastostatics and Laplace' equation [24]. Thus, having a look at the double layer kernel function with all arguments skipped

$$\begin{aligned}\left(\hat{\mathcal{T}}_{\mathbf{y}}\hat{\mathbf{U}}\right)^{\top} &= \left[\begin{bmatrix} \hat{\mathcal{T}}^{e}_{\mathbf{y}} & s\alpha\mathbf{n}_{\mathbf{y}} \\ -\beta\mathbf{n}_{\mathbf{y}}^{\top} & \frac{\beta}{s\rho_0^f}\mathbf{n}_{\mathbf{y}}^{\top}\nabla_{\mathbf{y}} \end{bmatrix} \begin{bmatrix} \hat{\mathbf{U}}^{s} & \hat{\mathbf{U}}^{f} \\ \left(\hat{\mathbf{P}}^{s}\right)^{\top} & \hat{P}^{f} \end{bmatrix}\right]^{\top} \\ &= \begin{bmatrix} \hat{\mathbf{T}}^{s} & \hat{\mathbf{T}}^{f} \\ \left(\hat{\mathbf{Q}}^{s}\right)^{\top} & \hat{Q}^{f} \end{bmatrix}^{\top},\end{aligned} \tag{22}$$

reveals that the same holds there as well, i.e., only the solid related part $\hat{\mathbf{T}}^{s}$ becomes strongly singular due to the application of $\hat{\mathcal{T}}^{e}_{\mathbf{y}}$ onto $\hat{\mathbf{U}}^{s}$. This observation is easily verified by means of a decomposition of $\hat{\mathbf{U}}^{s}$ into a singular and a regular part, respectively

$$\begin{aligned}\hat{\mathbf{U}}^{s}(r) =& \hat{\mathbf{U}}^{s}_{sing}(r) + \hat{\mathbf{U}}^{s}_{reg}(r) \quad \text{with} \quad r := |\mathbf{y}-\mathbf{x}| \\ =& \frac{1}{\mu}\left[\mathbf{I}\Delta_{\mathbf{y}} - \frac{\lambda+\mu}{\lambda+2\mu}\nabla_{\mathbf{y}}\nabla_{\mathbf{y}}^{\top}\right]\Delta_{\mathbf{y}}\hat{\chi}(r) \\ & - \frac{1}{\mu}\Big[\left(\left(k_1^2+k_2^2\right)\Delta_{\mathbf{y}} - k_1^2k_2^2\right)\mathbf{I} \\ & - \left(k_1^2+k_2^2-k_4^2-\frac{k_1^2k_2^2}{k_3^2}\right)\nabla_{\mathbf{y}}\nabla_{\mathbf{y}}^{\top}\Big]\hat{\chi}(r)\,,\end{aligned} \tag{23}$$

with the definitions of k_1, k_2, k_3, k_4 and $\hat{\chi}(r)$ given in appendix A.1. $\hat{\mathbf{U}}^{s}_{sing}$ is explicitely given in the second line above and contains forth order derivatives of $\hat{\chi}(r)$, which are of $O\left(r^{-1}\right)$, whereas $\hat{\mathbf{U}}^{s}_{reg}$ one line below contains up to at most second order derivatives of $\hat{\chi}(r)$, which are of $O\left(r^{1}\right)$. Note that $\hat{\mathbf{U}}^{s}_{sing}$ not only contains the singularity of linear elastostatics as already mentioned before, but has the appropriate structure as required for the regularization procedure as well.

Contrary to $\hat{\mathbf{T}}^{s}$, the second term on the main diagonal $\hat{Q}^{f}$, i.e., the application of the normal derivative onto $\hat{P}^{f}$, does not lead to a strong singularity for smooth enough surfaces [9]. Moreover, the off diagonal terms do not need any treatment either, as can be verified by having a look at the definition of the fundamental solution given in the appendix A.1. Due to this observation, only the regularization of the solid related part is worked out in detail, whereas the remaining terms of the double layer kernel can be found in [24].

Together with the central assumption of a closed boundary $\partial\Gamma = \{\emptyset\}$, Stokes theorem, and the definition of the skew symmetric Günter [14] differential operator $\mathcal{M}_{\mathbf{y}}$, the main ingredients for the regularization of $\hat{\mathbf{T}}^{s}$ are identified and can be found in appendix A.2. Here, only, the resulting integration by parts formulas are recalled for the later use

$$\int_{\Gamma} \left(\mathcal{M}_{\mathbf{y}}\, v\right)\mathbf{u}\,\mathrm{d}s_{\mathbf{y}} = -\int_{\Gamma} v\left(\mathcal{M}_{\mathbf{y}}\,\mathbf{u}\right)\mathrm{d}s_{\mathbf{y}} \tag{24}$$

$$\int_{\Gamma} \left(\mathcal{M}_{\mathbf{y}}\,\mathbf{v}\right)^{\top}\mathbf{u}\,\mathrm{d}s_{\mathbf{y}} = \int_{\Gamma} \mathbf{v}^{\top}\left(\mathcal{M}_{\mathbf{y}}\,\mathbf{u}\right)\mathrm{d}s_{\mathbf{y}}\,. \tag{25}$$

Next, writing $\hat{\mathbf{T}}^s$ (22) out in more detail together with the before introduced decomposition (23), results in the following representation of the solid related double layer kernel

$$\begin{aligned}\left(\hat{\mathbf{T}}^s\right)^\top &= \left(\mathcal{T}_{\mathbf{y}}^e\left(\hat{\mathbf{U}}_{sing}^s + \hat{\mathbf{U}}_{reg}^s\right)\right)^\top + s\alpha\hat{\mathbf{P}}^s\mathbf{n}_{\mathbf{y}}^\top \\ &= \left(\mathcal{T}_{\mathbf{y}}^e\hat{\mathbf{U}}_{sing}^s\right)^\top + O(r^0)\,.\end{aligned} \tag{26}$$

Introducing the same representation of $\mathcal{T}_{\mathbf{y}}^e$ as in [14], this rewrites as

$$\left(\hat{\mathbf{T}}^s\right)^\top = (\lambda+2\mu)\,\mathbf{n}_{\mathbf{y}}\nabla_{\mathbf{y}}^\top\hat{\mathbf{U}}_{sing}^s - \mu\left(\mathbf{n}_{\mathbf{y}}\times\left(\nabla_{\mathbf{y}}\times\hat{\mathbf{U}}_{sing}^s\right)\right) + 2\mu\mathcal{M}_{\mathbf{y}}\hat{\mathbf{U}}_{sing}^s + O(r^0)\,, \tag{27}$$

which for the structure of $\hat{\mathbf{U}}_{sing}^s$ given in (23) can be rearranged to

$$\left(\hat{\mathbf{T}}^s\right)^\top = \mathcal{M}_{\mathbf{y}}\Delta_{\mathbf{y}}^2\hat{\boldsymbol{\chi}} + \mathbf{I}\left(\mathbf{n}^\top\nabla_{\mathbf{y}}\right)\Delta_{\mathbf{y}}^2\hat{\boldsymbol{\chi}} + 2\mu\left(\mathcal{M}_{\mathbf{y}}\hat{\mathbf{U}}_{sing}^s\right)^\top + O(r^0)\,. \tag{28}$$

This is already the desired form of the kernel function, which is suitable for integration by parts. Plugging (28) into the definition of (13)

$$\left(\hat{\mathcal{K}}\hat{\mathbf{u}}\right)_\Omega^s(\tilde{\mathbf{x}}) = \int_\Gamma\left[\left(\mathcal{M}_{\mathbf{y}}\Delta_{\mathbf{y}}^2\hat{\boldsymbol{\chi}}\right)\hat{\mathbf{u}} + \left(\mathbf{I}\left(\mathbf{n}^\top\nabla_{\mathbf{y}}\right)\Delta_{\mathbf{y}}^2\hat{\boldsymbol{\chi}}\right)\hat{\mathbf{u}} + 2\mu\left(\mathcal{M}_{\mathbf{y}}\hat{\mathbf{U}}_{sing}^s\right)^\top\hat{\mathbf{u}} + O(r^0)\hat{\mathbf{u}}\right]\mathrm{d}s_{\mathbf{y}}\,, \tag{29}$$

the regularization can be performed by application of (24) to the first term on the right hand side and (25) to the third term, respectively. Keeping the symmetry of $\hat{\mathbf{U}}_{sing}^s$ in mind, this yields

$$\left(\hat{\mathcal{K}}\hat{\mathbf{u}}\right)_\Omega^s(\tilde{\mathbf{x}}) = \int_\Gamma\left[-\Delta_{\mathbf{y}}^2\hat{\boldsymbol{\chi}}\left(\mathcal{M}_{\mathbf{y}}\hat{\mathbf{u}}\right) + \left(\mathbf{I}\left(\mathbf{n}^\top\nabla_{\mathbf{y}}\right)\Delta_{\mathbf{y}}^2\hat{\boldsymbol{\chi}}\right)\hat{\mathbf{u}} + 2\mu\hat{\mathbf{U}}_{sing}^s\left(\mathcal{M}_{\mathbf{y}}\hat{\mathbf{u}}\right) + O(r^0)\hat{\mathbf{u}}\right]\mathrm{d}s_{\mathbf{y}}\,, \tag{30}$$

which is an equivalent form of the operator (13) under the assumption of a closed boundary.

What has to be done next, is the limit $\Omega\ni\tilde{\mathbf{x}}\to\mathbf{x}\in\Gamma$, which due to the before performed regularization is rather straightforward. For the last integral on the right hand side of (30) this limit poses no problem. Moreover, since the first and the third integrals on the right hand side of (30) have weakly singular kernel functions, they can continuously be extended to the boundary as well. The only part, which needs to be investigated, is the second term containing the normal derivative of $\Delta_{\mathbf{y}}^2\hat{\boldsymbol{\chi}}$. However, with

$$\left(\mathbf{n}^\top\nabla_{\mathbf{y}}\right)\Delta_{\mathbf{y}}^2\hat{\boldsymbol{\chi}}(r) = \frac{\mathbf{n}^\top\nabla_{\mathbf{y}}r}{4\pi r^2} + O\left(r^0\right) \tag{31}$$

the solid related jump term $\mathcal{C}^s(\mathbf{x})$ reduces to the jump term of Laplace' equation $c(\mathbf{x})$

$$\mathcal{C}^s(\mathbf{x}) = I(\mathbf{x})\,c(\mathbf{x}) \quad \text{with} \quad c(\mathbf{x}) = \frac{\Phi(\mathbf{x})}{4\pi}\,, \tag{32}$$

where $\Phi(\mathbf{x})$ is the internal solid angle, which may be computed as presented by Mantic [18]. Due to the regularization, the jump term becomes a constant only depending on the geometry, i.e., does neither depend on the material nor on the Laplace parameter s. Therefore, the solid related part of the limit (16) finally becomes

$$\lim_{\Omega\ni\tilde{\mathbf{x}}\to\mathbf{x}\in\Gamma}\left(\hat{\mathcal{K}}\hat{\mathbf{u}}\right)_\Omega^s(\tilde{\mathbf{x}}) = -I(\mathbf{x})\left[-1+c(\mathbf{x})\right]\hat{\mathbf{u}}(\mathbf{x}) + \left(\hat{\mathcal{K}}\hat{\mathbf{u}}\right)^s(\mathbf{x})\,, \tag{33}$$

with the regularized double layer kernel function (30).

Remark 1 Stressing the assumption of a closed boundary once again, for the implementation a more efficient form of (30) is found, which is obtained by augmenting $\hat{\mathbf{U}}^s_{sing}$ to $\hat{\mathbf{U}}^s$. This is done by adding and subtracting the regular part, making use of (25)

$$\left(\hat{\mathcal{K}}\hat{\mathbf{u}}\right)^s_\Omega(\tilde{\mathbf{x}}) = \int_\Gamma \Big[-\Delta^2_{\mathbf{y}}\hat{\chi}\left(\mathcal{M}_{\mathbf{y}}\hat{\mathbf{u}}\right) + \left(\mathbf{I}\left(\mathbf{n}^\top\nabla_{\mathbf{y}}\right)\Delta^2_{\mathbf{y}}\hat{\chi}\right)\hat{\mathbf{u}} + 2\mu\hat{\mathbf{U}}^s\left(\mathcal{M}_{\mathbf{y}}\hat{\mathbf{u}}\right) + O\left(r^0\right)\hat{\mathbf{u}}\Big]\mathrm{d}s_y \,. \tag{34}$$

Since this modification only concerns regular parts of the operator, the jump term is not affected at all.

Remark 2 The just performed regularization still requires the evaluation of weakly singular integral operators. Within a numerical scheme it does not suffice to just use standard Gaussian quadrature, thus in the presented approach, beforehand a Duffy transformation [28] is performed.

3.3 Temporal Discretization

Before the CQM is applied to the convolution operator in (20), its application to (21) is presented. Splitting the time interval $(0,T)$ into $N+1$ equidistant time steps Δt, the convolution at a discrete time $t_n = n\Delta t$ is approximated by the quadrature rule

$$(f*g)(t_n) \approx \sum_{k=0}^{n} \omega^{\Delta t}_{n-k}(\hat{f})\, g(t_k) \,. \tag{35}$$

The derivation of the quadrature weights can be found in [15], whereas here they are assumed to be given by definition

$$\omega^{\Delta t}_n(\hat{f}) := \frac{1}{2\pi i}\oint \hat{f}\left(\frac{\gamma(z)}{\Delta t}\right) z^{-(n+1)}\mathrm{d}z \,. \tag{36}$$

For their computation, the closed contour has to lie entirely in the domain of analyticity of $\hat{f}$, but can be chosen of any shape otherwise. Choosing it to be a circle centered at the origin with radius $\mathscr{R}$, parameterized by a polar coordinate transformation $z = \mathscr{R}\mathrm{e}^{-i\varphi}$, allows to approximate the integral (36) with the trapezoidal rule for $L+1$ equal steps

$$\begin{aligned} \omega^{\Delta t}_n(\hat{f}) \approx & \frac{\mathscr{R}^{-n}}{L+1}\sum_{\ell=0}^{L}\hat{f}\left(s_\ell\right)\zeta^{\ell n} \\ & \text{with} \quad \zeta = \mathrm{e}^{\frac{2\pi i}{L+1}} \quad \text{and} \quad s_\ell = \frac{\gamma(\mathscr{R}\zeta^{-\ell})}{\Delta t} \,, \end{aligned} \tag{37}$$

where γ is the quotient of the characteristic polynomials resulting from the underlying linear multi-step method [15]. The next steps follow the procedure as outlined in [1], thus plugging (37) into (35), extending the outer sum to $k = N$, assuming $L = N$, and setting $\omega^{\Delta t}_k = 0$ for

negative indices due to causality, results in

$$\begin{aligned}(f*g)(t_n) &\approx \sum_{k=0}^{N} \frac{\mathscr{R}^{-(n-k)}}{N+1} \sum_{\ell=0}^{N} \hat{f}(s_\ell)\, \zeta^{\ell(n-k)}\, g(t_k) \\ &\approx \frac{\mathscr{R}^{-n}}{N+1} \sum_{\ell=0}^{N} \hat{f}(s_\ell)\, \hat{g}(s_\ell)\, \zeta^{\ell n} \\ &\text{with} \quad \hat{g}(s_\ell) = \sum_{k=0}^{N} \mathscr{R}^k g(t_k) \zeta^{-\ell k}\,. \end{aligned} \tag{38}$$

It is easily verified that exchanging the summation order of the finite double sum leaves the final result unchanged. Applying this procedure to the convolution operator of the original problem (20)

$$\mathcal{C}(\mathbf{x})\mathbf{u}^g(\mathbf{x},t) = (\mathcal{V} * \mathbf{t}^g)(\mathbf{x},t) - (\mathcal{K} * \mathbf{u}^g)(\mathbf{x},t)\,, \tag{39}$$

yields a set of $N+1$ Laplace domain problems to be discretized in space

$$\mathcal{C}(\mathbf{x})\hat{\mathbf{u}}^g(\mathbf{x},s_\ell) = \left(\hat{\mathcal{V}}\hat{\mathbf{t}}^g\right)(\mathbf{x},s_\ell) - \left(\hat{\mathcal{K}}\hat{\mathbf{u}}^g\right)(\mathbf{x},s_\ell) \quad \ell = 0\ldots N\,. \tag{40}$$

Time domain results for the original problem, are obtained via the formula in the final line of (38). From an engineering point of view, a more detailed presentation of this technique may be found in [26].

3.4 Spatial Discretization

The computational domain $\Gamma = \partial\Omega$ is approximated via a standard triangulation by the union of M triangles τ_m

$$\Gamma \approx \Gamma_h = \bigcup_{m=1}^{M} \tau_m\,. \tag{41}$$

For the sought after solutions of (40), the following subspaces on Γ_h are defined

$$S_h[k](\Gamma_{N,h}) := \text{span}\{\varphi_i^\alpha[k]\}_{i=1}^{I} \tag{42}$$

$$S_h[k](\Gamma_{D,h}) := \text{span}\{\psi_j^\beta[k]\}_{j=1}^{J}\,, \tag{43}$$

where $k = 1\ldots4$ are the four poroelastic degrees of freedom, and i and j the nodes on the Neumann, respectively the Dirichlet boundary. The unknown Dirichlet datum is approximated by a linear combination of I continuous polynomial shape functions $\varphi_i^\alpha[k]$ of order $\alpha \geq 1$, which ensures a meaningful regularized double layer operator (30). Contrary, the J piecewise discontinuous polynomial shape functions $\psi_j^\beta[k]$ of order $\beta \geq 0$ are used to approximate the unknown Neumann datum

$$\hat{\mathbf{u}}^g[k](\mathbf{x}) \approx \hat{\mathbf{u}}_h^g[k](\mathbf{x}) = \sum_{i=1}^{I} \hat{\mathrm{u}}_{\mathrm{h,i}}^{\mathrm{g}}[k]\varphi_i^\alpha[k](\mathbf{x}) \in S_h[k](\Gamma_{N,h}) \tag{44}$$

$$\hat{\mathbf{t}}^g[k](\mathbf{x}) \approx \hat{\mathbf{t}}_h^g[k](\mathbf{x}) = \sum_{j=1}^{J} \hat{\mathrm{t}}_{\mathrm{h,j}}^{\mathrm{g}}[k]\psi_j^\beta[k](\mathbf{x}) \in S_h[k](\Gamma_{D,h})\,. \tag{45}$$

Plugging these approximations into (40), yields $N+1$ equations with $(I+J)\times 4$ unknowns each. Claiming these equations to be satisfied at J collocation points on the Dirichlet boundary and I collocation points on the Neumann boundary, yields $N+1$ algebraic systems of equations, which are solvable for pairwise different collocation points. On the Neumann boundary, the obvious choice is to make them coincide with the nodes, whereas on the Dirichlet boundary the matter is a little more complicated. Since discontinuous elements' nodes coincide for neighboring elements, this choice does in general not deliver linear independent equations. This matter is solved by indenting the collocation points with respect to the nodes, such that their geometrical position becomes unique, as it is required for all collocation points. With the introduced discretization and this choice of collocation points, the ℓ^{th} system of equations reads as

$$\begin{bmatrix} \hat{\mathsf{V}}_{\mathsf{DD}} & -\hat{\mathsf{K}}_{\mathsf{DN}} \\ \hat{\mathsf{V}}_{\mathsf{ND}} & -(\mathsf{C}+\hat{\mathsf{K}}_{\mathsf{NN}}) \end{bmatrix}_{\ell} \begin{bmatrix} \hat{\mathsf{t}}^{\mathsf{g}}_{\mathsf{D,h}} \\ \hat{\mathsf{u}}^{\mathsf{g}}_{\mathsf{N,h}} \end{bmatrix}_{\ell} = \begin{bmatrix} -\hat{\mathsf{V}}_{\mathsf{DN}} & (\mathsf{C}+\hat{\mathsf{K}}_{\mathsf{DD}}) \\ -\hat{\mathsf{V}}_{\mathsf{NN}} & \hat{\mathsf{K}}_{\mathsf{ND}} \end{bmatrix}_{\ell} \begin{bmatrix} \hat{\mathsf{g}}^{\mathsf{g}}_{\mathsf{N,h}} \\ \hat{\mathsf{g}}^{\mathsf{g}}_{\mathsf{D,h}} \end{bmatrix}_{\ell} \quad \ell = 0 \ldots N \,. \tag{46}$$

Upper case subscripts indicate the boundaries, which the vectors and matrices are related to and, therewith, also their dimension. Note that due to the block structure of the system matrix, a Schur complement can be defined

$$\hat{\mathsf{S}}_{\mathsf{NN}} := \hat{\mathsf{V}}_{\mathsf{ND}} \hat{\mathsf{V}}_{\mathsf{DD}}^{-1} \hat{\mathsf{K}}_{\mathsf{DN}} - (\mathsf{C}+\hat{\mathsf{K}}_{\mathsf{NN}}) \,, \tag{47}$$

which is used within the solution procedure for the linear systems of equations, either with a direct or indirect solver.

4 Numerical Examples

In both examples presented in this section, for the underlying linear multi-step method within the CQM, the BDF2 is chosen. The Dirichlet datum is continuously approximated by piecewise linear and the Neumann datum discontinuously by piecewise constant shape functions. The relevant material data are given in Table1. All computations have been performed by using the HyENA C++ library for solving partial differential equations using boundary element methods [21].

Table 1: Material data for rock (Berea sandstone) and a sandy soil [13]

	rock	soil
$\lambda\,[\mathrm{N/m^2}]$	0	$1.44\cdot 10^8$
$\mu\,[\mathrm{N/m^2}]$	$7.2\cdot 10^9$	$9.78\cdot 10^7$
$\rho\,[\mathrm{kg/m^3}]$	2458	1884
$\phi\,[-]$	0.19	0.48
$\alpha\,[\mathrm{N/m^2}]$	0.778	0.981
$\rho^f\,[\mathrm{kg/m^3}]$	1000	1000
$R\,[\mathrm{N/m^2}]$	$4.885\cdot 10^8$	$1.206\cdot 10^9$
$\kappa\,[\mathrm{m^4/Ns}]$	$1.9\cdot 10^{-10}$	$3.5\cdot 10^{-9}$

4.1 Wave Propagation in a 1D-Column

For sake of validation, wave propagation in a one-dimensional column is studied and the obtained results are compared with the semi-analytic solution by Schanz and Cheng [27]. A closed form of the time domain reference solution is in general not possible, but can only be obtained numerically - in this case via CQM. A column with length $\ell = 3\,\mathrm{m}$ times a cross sectional area

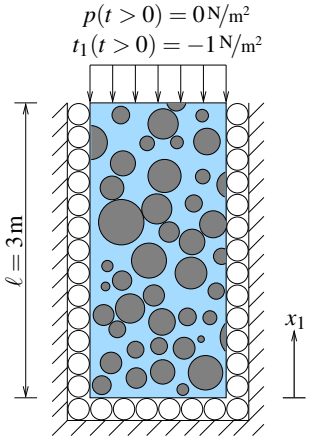

Figure 1: Poroelastic column

of $A = 1\,\mathrm{m} \times 1\,\mathrm{m}$ is considered (Figure1). To come as close as possible to the one-dimensional case, the surrounding sidewalls and the bottom face of the column are supported by impermeable roller bearings, i.e., zero normal displacement and no flux are allowed to happen, whereas in-plane motion is not restricted at all. The top face of the column is subjected to a step stress load in normal direction of $t_1 = -1\,\mathrm{N/m^2}$ for $t > 0$ and zero pressure at all times. Furthermore, material data of rock (Table1), with Poisson's ratio artificially set to zero are used, resulting in $\lambda = 0$.

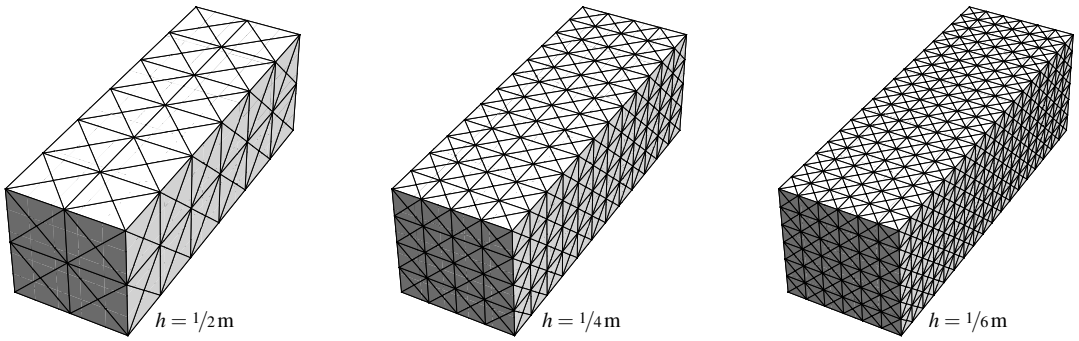

(a) COL1 (b) COL2 (c) COL3

Figure 2: Different spatial discretizations of the considered column

Introducing the dimensionless *Courant-Friedrichs-Levy* number β_{CFL}

$$\beta_{\text{CFL}} := \frac{c_1 \Delta t}{h} , \tag{48}$$

allows to compare different spatial and temporal discretizations. In the definition above, c_1 is the fast compression wave speed for $t \to 0$, Δt the chosen time step, and h marks the mesh size, which is defined to be equal to the triangles' hypotenuses. The different meshes used are depicted in Figure2 and characterized as follows: COL1 has 224 elements and 114 nodes, COL2 consists of 896 elements and 450 nodes, and COL3 is made up by 2016 elements on 1010 nodes.

Figure3 and Figure4 show displacment and stress results for the solid, respectively pressure and flux results for the fluid phase with $\beta_{\text{CFL}} = 0.3$ (its influence is studied afterwards, where one can see that values between 0.125 and 0.5 yield good results). The displacement u_1 at the center of the top face and the flux q through it are plotted in Figure3(a) and Figure4(b), respectively. The traction results t_1 and the pressure p in Figure3(b) and Figure4(a) are observed at the midpoint of the bottom face. These results show that COL1 is to coarse and COL3 obviously delivers the best results. However, COL2 gives satisfactory results as well, which is why this mesh is chosen next to study the influence of the β_{CFL} number.

For lower β_{CFL} values (more elements per wave length) the CQM tends to become less stable, whereas for higher values (less elements per wave length) the numerical damping increases more and more. These observations are confirmed by Figure5. There, again a one-dimensional wave propagation is investigated, however, now keeping the spatial discretization constant (COL2) and varying β_{CFL} by changing the time step Δt. While in Figure5(a) instability of the displacement results is not visible for the lowest β_{CFL} value, the traction results in Figure5(b) start to become unstable even at the next higher β_{CFL} value (for sake of visibility not the whole range is plotted). On the other side, the displacement results clearly show the damping at higher β_{CFL} values. Commenting on the skipped results, the fluid pressure essentially behaves the same as the solid traction, whereas the flux becomes even more unstable for lower β_{CFL} values, than the traction results.

A problem, frequently attributed to collocation methods, is the lack of long time stability compared to other methods, such as Galerkin type approaches. However, some long time computations have shown that with the collocation formulation chosen in this work, this problem does not seem to be as significant, as reported in [11] for the the same problem in linear elasticity. The long time result for the fluid pressure behaves almost identical to the traction solution depicted in Figure6, whereas the result for the solid displacement seem to behave a little better and the flux result is marginally worse in quality.

Remark 3 A novelty of this boundary element formulation is that poroelastodynamic flux results can be computed, e.g., Figure3(a). Such results have not yet been reported in literature.

4.2 Wave Propagation in a Half-space

The case of a poroelastic half-space is considered next. In the engineering community, this is a classical problem to be studied with boundary elements. When dealing with such a domain,

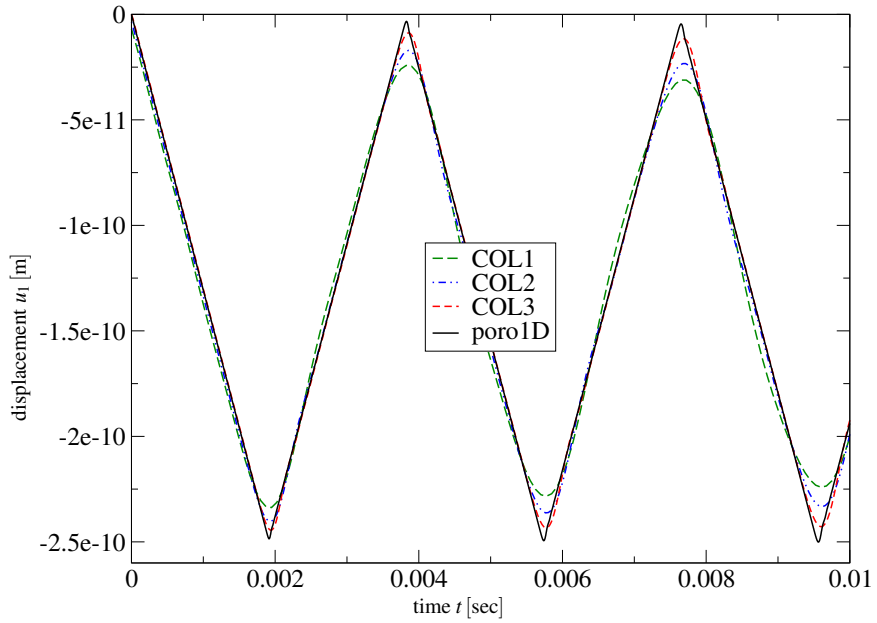

(a) Solid displacement u_1

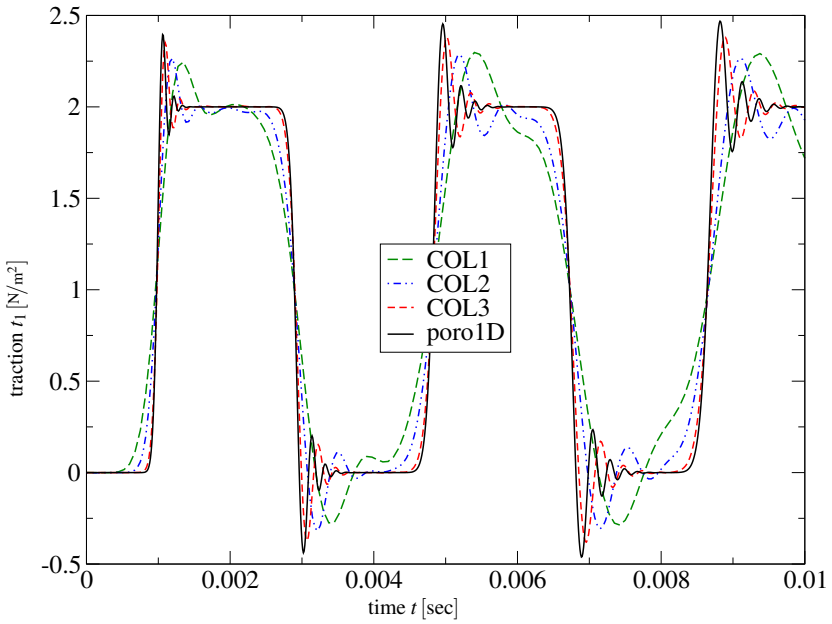

(b) Solid traction t_1

Figure 3: Solid displacement and traction results for $\beta_{\text{CFL}} = 0.3$ compared with the semi-analytic solution

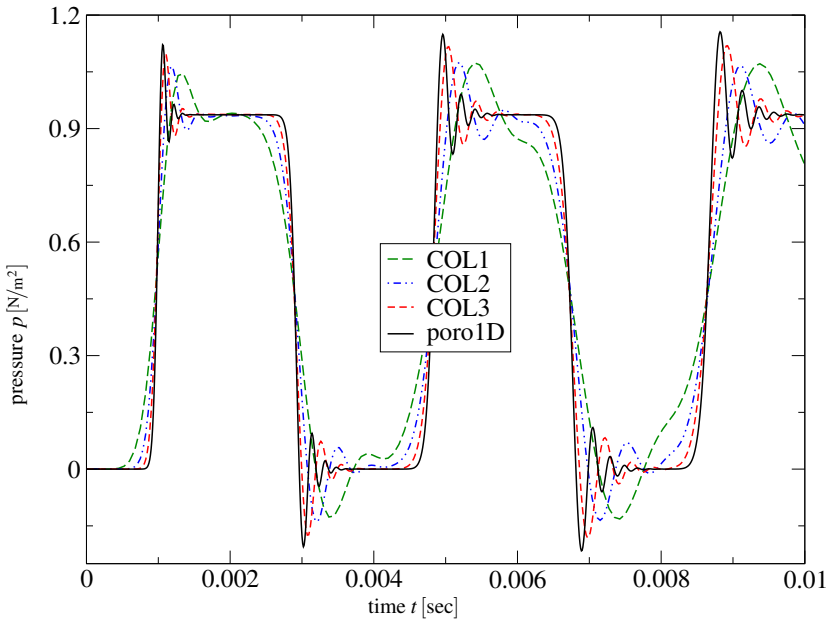

(a) Fluid pressure p

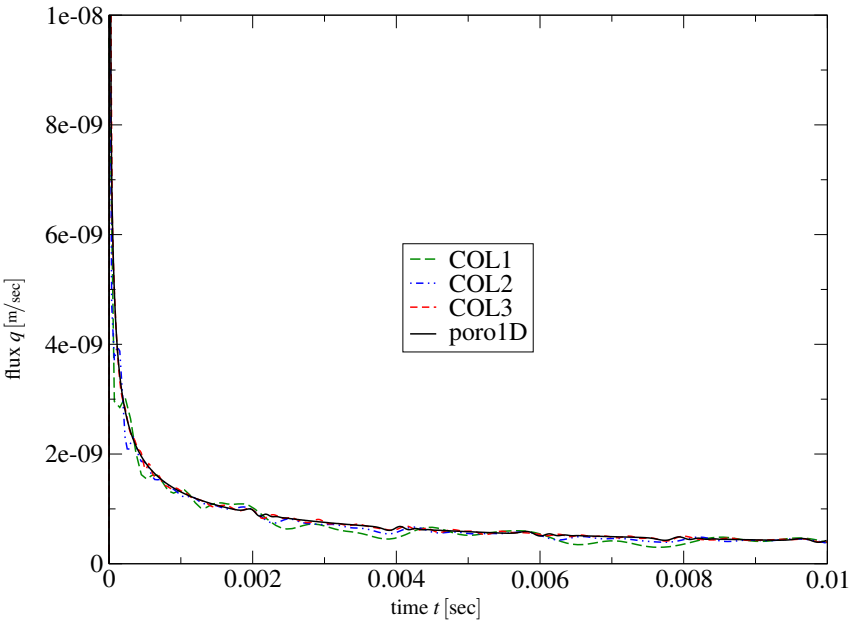

(b) Fluid flux q

Figure 4: Fluid pressure and flux results for $\beta_{\text{CFL}} = 0.3$ compared with the semi-analytic solution

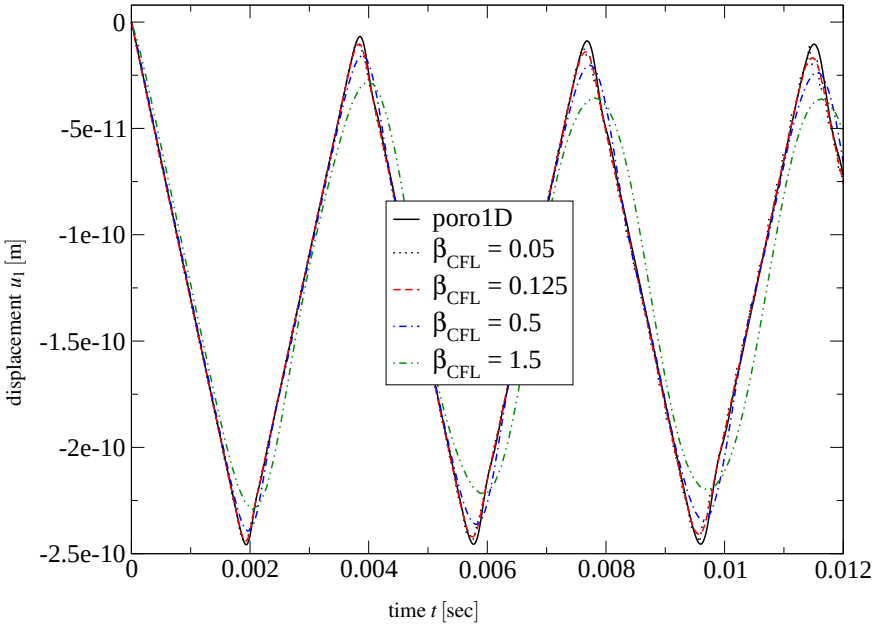

(a) Solid displacement u_1

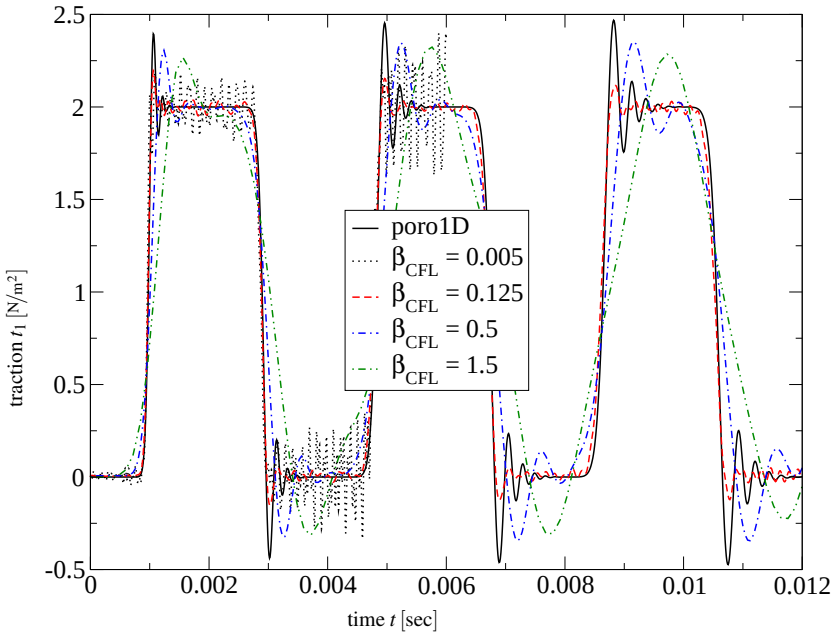

(b) Solid traction t_1

Figure 5: Comparison of different time steps (β_{CFL} values) for COL2

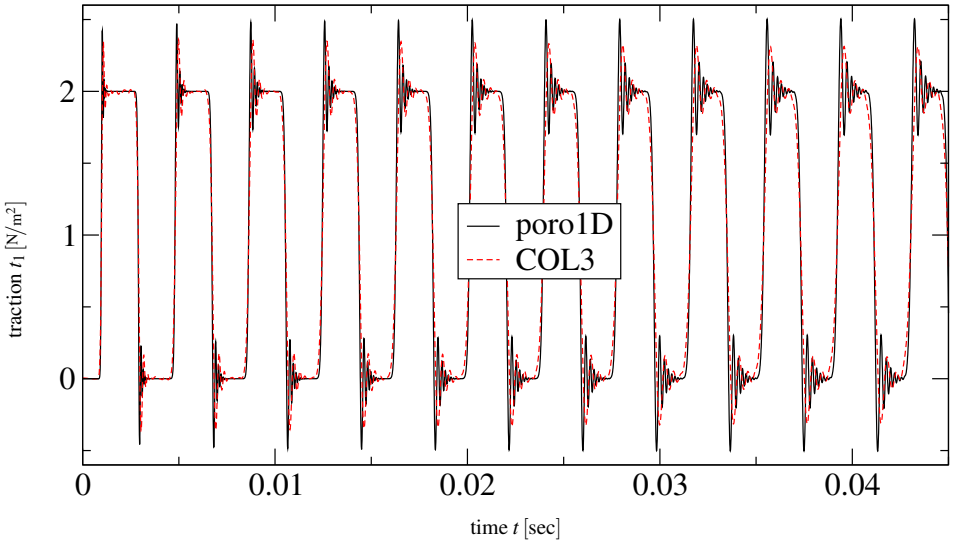

Figure 6: Long time traction solution for $\beta_{\text{CFL}} = 0.3$

two obvious error sources are introduced: First, the discretization error due to the necessary truncation of the infinite boundary at some finite extent as depicted in Figure7 and, second, the implication this truncation has on the double layer operator. This results in violation of its definition as a Cauchy principal value in the classical formulation, or in a violation of the assumption of a closed boundary within the here presented approach. Note that this error is strictly due to the discretization, on the continuous level, where the regularization was performed, $\partial\Gamma = \{\emptyset\}$ still holds for the half-space, too.

Comparing the results obtained by the here presented approach with results by Schanz [24], shows that they are of at least the same quality. Schanz also developed a CQM based collocation BEM, however there the double layer operator is evaluated numerically [8] and, furthermore, all data are continuously approximated by piece-wise linear shape functions with double nodes taking care of discontinuities.

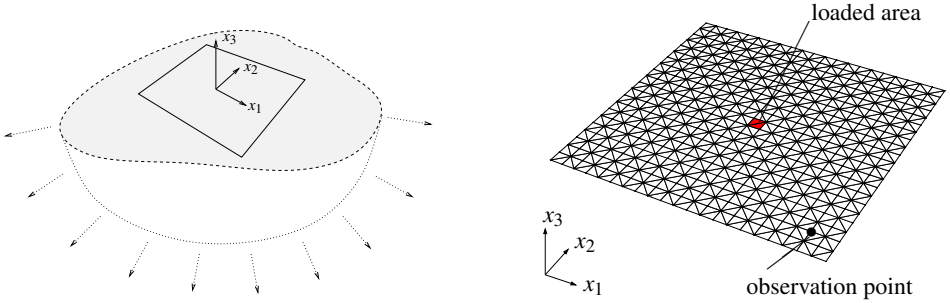

(a) Half-space (b) Mesh

Figure 7: Half-space with a finite discretization

The discretized half-space in Figure7 is a flat patch of $10\,\mathrm{m} \times 10\,\mathrm{m}$ using a triangulation with 484 nodes and 882 regular triangles, which outer normal points in the positive x_3-direction. For the material data, properties of soil as listed in Table1 are assumed. The marked area of $0.476\,\mathrm{m} \times 0.476\,\mathrm{m}$ at the center in Figure7(b) is loaded with a traction step load of $t_3 = -1\,\mathrm{N/m^2}$ for $t > 0$, whereas all remaining elements are traction free. Furthermore, zero pressure is applied on the entire surface. The observation point for the vertical displacement u_3 is located on the diagonal at 5.39 m from the loaded area. The results are depicted in Figure8 versus time.

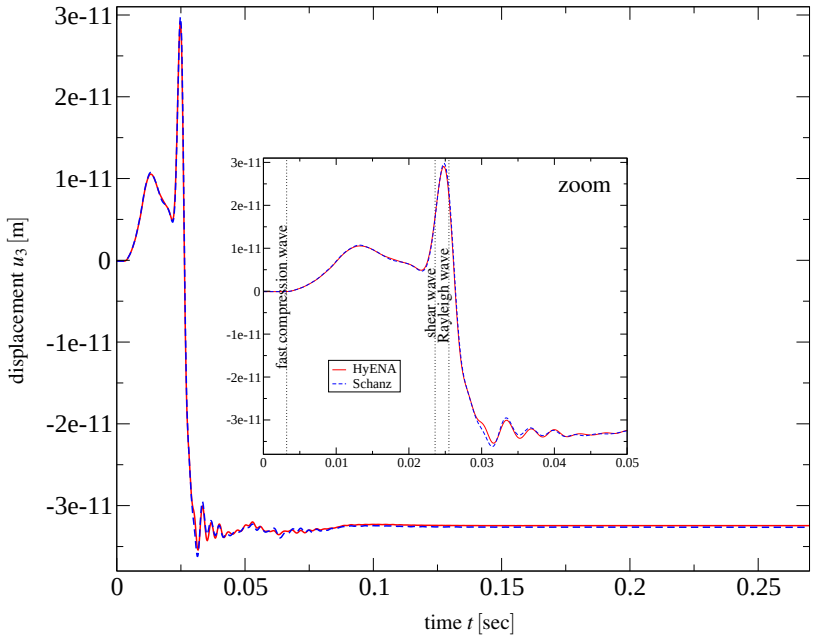

Figure 8: Vertical displacement u_3 at the observation point versus time ($\beta_{\mathrm{CFL}} = 0.5$)

The arrival time of the fast compression wave at the observation point computes to $t = 0.0032\,\mathrm{sec}$, which is in rather good agreement with the BEM results, whereas the slow compression wave is not visible for the given material parameters. Due to the similar wave speed of the shear- and the Rayleigh wave, a distinction at such a short distance is not possible, which makes the identification of their arrival times impossible. Nevertheless, their computed arrival times are marked in Figure8.

The oscillation after all waves have passed results from the CQM, which is as nearly all time stepping techniques not capable to resolve jumps. Computing the arrival time of the reflected Rayleigh wave from the most distant point, results in $t = 0.096\,\mathrm{sec}$. In Figure8, one can observe that at this time the solution reaches already a static value. The explanation for this phenomenon are slight reflections on the truncation, which however, are highly damped. In fact, multiple oscillations can not be observed at all.

Remark 4 The first example was computed using the regularized version of the double layer operator (34) mentioned in Remark 1. However, the additional modification mentioned therein,

seems to affect the half-space solution too much (the assumption of a closed boundary is violated), which is why the computation of the second example was performed using (30).

5 Conclusions

Based on Biot's theory a regularized double layer operator for the u,p formulation in Laplace domain has been derived. As a result of integration by parts a weakly singular representation of the first boundary integral equation was obtained, starting from where a CQM based collocation BEM was established.

At this point it should be pointed out that neither the collocation scheme, nor the CQM are restrictions to the used regularization technique, since it is performed on a continuous level. In fact, the resulting weakly singular first boundary integral equation can also be used within a Galerkin scheme, too. Furthermore, since the regularization technique was used to remove the strong singularity inherited from linear elastostatics, the proposed method must also work for other formulations than the one presented in this article, e.g., all poroelastic BEM formulations listed in the introduction. Additionally, since this regularization technique is just an intermediate result of the hypersingular operator's regularization, an extension to a symmetric Galerkin formulation comes along quite naturally.

The major assumption within the applied regularization technique was the requirement of domains with closed boundary. This restriction is a consequence of Stokes theorem on which the whole technique relies. However, the numerical example considering the poroelastic half-space shows that disregarding the violation of this assumption the results are of at least the same quality as obtained with other formulations found in literature.

Together with the point-wise evaluation of the jump term within the framework of the presented weakly singular first boundary integral equation, the proposed collocation scheme allows a flexible approximation of the Cauchy data with basically any meaningful combination of trial spaces and choice of collocation points. In the way it was presented here, a system matrix with block structure results, which maintains the physical properties of the operators.

As a final remark one may note that the proposed method also works for linear elasticity and viscoelasticity, since there one has to deal with the same singularity.

Acknowledgement The authors gratefully acknowledge the financial support of the Austrian Science Fund (FWF) within the *Doktoratskolleg W1208 – Numerical Simulations in Technical Science*.

A Appendix

A.1 Poroelastodynamic Fundamental Solution

The Laplace domain fundamental solution

$$\hat{\mathbf{U}}(r) = \begin{bmatrix} \hat{\mathbf{U}}^s(r) & \hat{\mathbf{U}}^f(r) \\ \left(\hat{\mathbf{P}}^s\right)^\top(r) & \hat{P}^f(r) \end{bmatrix} \quad \text{with} \quad r := |\mathbf{y}-\mathbf{y}| \tag{49}$$

is recalled from [24]. There, the solid displacement related part of the fundamental solution is given as

$$\begin{aligned}
\hat{\mathbf{U}}^s =& \frac{1}{4\pi r(\rho-\beta\rho^f)}\left[\mathbf{R}_1\frac{k_4^2-k_2^2}{k_1^2-k_2^2}\mathrm{e}^{-k_1 r}-\mathbf{R}_2\frac{k_4^2-k_1^2}{k_1^2-k_2^2}\mathrm{e}^{-k_2 r}+\left(\mathbf{I}k_3^2-\mathbf{R}_3\right)\mathrm{e}^{-k_3 r}\right] \\
&\text{with}\quad \mathbf{R}_j=\frac{3\nabla r\,\nabla^\top r-\mathbf{I}}{r^2}+k_j\frac{3\nabla r\,\nabla^\top r-\mathbf{I}}{r}+k_j^2\nabla r\,\nabla^\top r \\
\hat{\mathbf{U}}^s =& \frac{1}{8\pi\mu r\,(\lambda+2\mu)}\left[(\lambda+\mu)\,\nabla r\nabla^\top r+\mathbf{I}\,(\lambda+3\mu)\right]+O\left(r^0\right)\ ,
\end{aligned} \tag{50}$$

where k_1, k_2, and k_3 are the wave numbers related to the fast/slow compressional, and the shear wave [24], whereas the abbreviation $k_4 = k_3\sqrt{\mu/\lambda+2\mu}$ is just introduced for notational convenience. For the regularization, however, a more suitable form of (50) is needed, which is obtained by the following decomposition

$$\begin{aligned}
\hat{\mathbf{U}}^s(r) =& \hat{\mathbf{U}}^s_{sing}(r)+\hat{\mathbf{U}}^s_{reg}(r)\quad \text{with}\quad r:=|\mathbf{y}-\mathbf{x}| \\
=& \frac{1}{\mu}\left[\mathbf{I}\Delta_{\mathbf{y}}-\frac{\lambda+\mu}{\lambda+2\mu}\nabla_{\mathbf{y}}\nabla_{\mathbf{y}}^\top\right]\Delta_{\mathbf{y}}\hat{\chi}(r) \\
&-\frac{1}{\mu}\Big[\left(\left(k_1^2+k_2^2\right)\Delta_{\mathbf{y}}-k_1^2k_2^2\right)\mathbf{I} \\
&-\left(k_1^2+k_2^2-k_4^2-\frac{k_1^2k_2^2}{k_3^2}\right)\nabla_{\mathbf{y}}\nabla_{\mathbf{y}}^\top\Big]\hat{\chi}(r)\ ,
\end{aligned} \tag{51}$$

with

$$\begin{aligned}
\hat{\chi}(r) =& \frac{1}{4\pi r}\left[\frac{\mathrm{e}^{-k_1 r}}{(k_2^2-k_1^2)(k_3^2-k_1^2)}+\frac{\mathrm{e}^{-k_2 r}}{(k_2^2-k_1^2)(k_2^2-k_3^2)}+\frac{\mathrm{e}^{-k_3 r}}{(k_1^2-k_3^2)(k_2^2-k_3^2)}\right] \\
=& -\frac{1}{4\pi\left(k_1^2-k_2^2\right)\left(k_1^2-k_3^2\right)\left(k_3^2-k_2^2\right)}+O\left(r^2\right)\ .
\end{aligned} \tag{52}$$

The remaining parts of (49) are defined as

$$\hat{\mathbf{U}}^f(r) = \frac{\rho^f(\alpha-\beta)\nabla_{\mathbf{y}}r}{4\pi r\beta(\lambda+2\mu)(k_1^2-k_2^2)}\left[\left(k_1+\frac{1}{r}\right)\mathrm{e}^{-k_1 r}-\left(k_2+\frac{1}{r}\right)\mathrm{e}^{-k_2 r}\right]=O\left(r^0\right) \tag{53}$$

$$\hat{\mathbf{P}}^s(r) = \frac{\hat{\mathbf{U}}^f(r)}{s}=O\left(r^0\right) \tag{54}$$

$$\begin{aligned}
\hat{P}^f(r) =& \frac{s\rho^f}{4\pi r\beta\left(k_1^2-k_2^2\right)}\left[(k_1^2-k_4^2)\mathrm{e}^{-k_1 r}-(k_2^2-k_4^2)\mathrm{e}^{-k_2 r}\right] \\
=& \frac{s\rho^f}{4\pi\beta r}+O\left(r^0\right)\ .
\end{aligned} \tag{55}$$

Even though (55) is weakly singular, the application of the traction operator (14) does not lead to a strong singularity [9] in the double layer kernel, thus no special representation of it is required.

A.2 Stokes Theorem and Integration by Part Formulas

In $\mathbb{R}^3$, Stokes theorem for a differentiable vector field $\mathbf{a}(\mathbf{y})$ with $\mathbf{y} \in \Gamma = \bar{\Omega} \setminus \Omega$ is given by

$$\int_{\Gamma} (\nabla_{\mathbf{y}} \times \mathbf{a}, \mathbf{n}_{\mathbf{y}}) \, \mathrm{d}s_{\mathbf{y}} = \int_{\partial\Gamma} (\mathbf{a}, \nu) \, \mathrm{d}\gamma_{\mathbf{y}} \,, \tag{56}$$

where ν is the unit tangent vector along the contour $\partial\Gamma$. Obviously, for a closed contour $\partial\Gamma = \{\emptyset\}$ the right hand side vanishes, which allows to rewrite (56) for this special case as

$$\int_{\Gamma} (\mathbf{n}_{\mathbf{y}} \times \nabla_{\mathbf{y}}, \mathbf{a}) \, \mathrm{d}s_{\mathbf{y}} = 0 \,. \tag{57}$$

With the definition of the Günter [14] derivative $\mathcal{M}_{\mathbf{y}} := \left(\mathbf{n}_{\mathbf{y}} \nabla_{\mathbf{y}}^{\top}\right)^{\top} - \mathbf{n}_{\mathbf{y}} \nabla_{\mathbf{y}}^{\top}$ from (57) the following formula can be derived

$$\int_{\Gamma} (\mathcal{M}_{\mathbf{y}} \, \mathbf{a}) \, \mathrm{d}s_{\mathbf{y}} = \mathbf{0} \,. \tag{58}$$

This formula is helpful for the derivation of the integration by part formulas [11] for the regularization of the double layer kernel function. Applying (58) to a vector $\mathbf{a} = v\mathbf{u}$ yields

$$\int_{\Gamma} (\mathcal{M}_{\mathbf{y}} \, v) \, \mathbf{u} \mathrm{d}s_{\mathbf{y}} = - \int_{\Gamma} v \, (\mathcal{M}_{\mathbf{y}} \, \mathbf{u}) \, \mathrm{d}s_{\mathbf{y}} \,, \tag{59}$$

and for the double contraction of $\mathcal{M}_{\mathbf{y}}$ with $\mathbf{u}\mathbf{v}^{\top}$

$$\int_{\Gamma} (\mathcal{M}_{\mathbf{y}} \, \mathbf{v})^{\top} \, \mathbf{u} \mathrm{d}s_{\mathbf{y}} = \int_{\Gamma} \mathbf{v}^{\top} \, (\mathcal{M}_{\mathbf{y}} \, \mathbf{u}) \, \mathrm{d}s_{\mathbf{y}} \tag{60}$$

is found.

References

[1] L. Banjai and S. Sauter. Rapid solution of the wave equation in unbounded domains. *Journal on Numerical Analysis*, 47(1):227–249109–128, 2008.

[2] E. Becache, J. C. Nedelec, and N. Nishimura. Regularization in 3D for anisotropic elastodynamic crack and obstacle problems. *Journal of Elasticity*, 31:25–46, 1993.

[3] M. A. Biot. Theory of propagation of elastic waves in a fluid-saturated porous solid. I. *Journal of the Acoustical Society of America*, 28(2):168–178, 1956.

[4] M. A. Biot. Theory of propagation of elastic waves in a fluid-saturated porous solid. II. *Journal of the Acoustical Society of America*, 28(2):179–191, 1956.

[5] G. Bonnet. Basic singular solutions for a poroelastic medium in the dynamic range. *Journal of the Acoustical Society of America*, 82(5):1758–1763, 1987.

[6] G. Bonnet and J. L. Auriault. *Dynamics of Saturated and Deformable Porous Media: Homogenization Theory and Determination of the Solid-Liquid Coupling Coefficients*, pages 306–316. Physics of Finely Divided Matter. Springer Verlag, Berlin, 1985.

[7] J. Chen and G. F. Dargush. Boundary element method for dynamic poroelastic and thermoelastic analyses. *International Journal for Solids and Structures*, 32(15):2257–2278, 1995.

[8] M. Guiggiani and A. Gigante. A general algorithm for multidimensional cauchy principal value integrals in the boundary element method. *Journal of Applied Mechanics*, 57:906–915, 1990.

[9] W. Hackbusch. *Integralgleichungen*. Teubner, 1989.

[10] H. Han. The boundary integro-differential equations of three-dimensional neumann problem in linear elasticity. *Numerische Mathematik*, 68:268–281, 1994.

[11] L. Kielhorn. *A Time-Domain Symmetric Galerkin BEM for Viscoelastodynamics.*, volume 5 of *Computation in Engineering and Science*. Verlag der Technischen Universtiät Graz, 2009.

[12] L. Kielhorn and M. Schanz. Convolution quadrature method-based symmetric Galerkin boundary element method for 3-d elastodynamics. *International Journal for Numerical Methods in Engineering*, 76:1724–1746, 2008.

[13] Y. K. Kim and H. B. Kingsbury. Dynamic characterization of poroelastic materials. *Experimental Mechanics*, 19:252–258, 1979.

[14] V. D. Kupradze. *Three-dimensional problems of the mathematical theory of elasticity and thermoelasticity*. North-Holland, 1979.

[15] C. Lubich. Convolution quadrature and discretized operational calculus I. *Numerische Mathematik*, 52:129–145, 1988.

[16] C. Lubich. Convolution quadrature and discretized operational calculus II. *Numerische Mathematik*, 52:413–425, 1988.

[17] G. D. Manolis and D. E. Beskos. Integral formulation and fundamental solutions of dynamic poroelasticity and thermoelasticity. *Acta Mechanica*, 76:89–104, 1989.

[18] V. Mantic. A new formula for the c-matrix in the somigliana identity. *Journal of Elasticity*, 33:191–201, 1993.

[19] P. A. Martin and F. J. Rizzo. On boundary integral equations for crack problems. *Proceedings of the Royal Society A*, 421(1861):341–335, 1989.

[20] A. W. Maue. Zur Formulierung eines allgemeinen Beugungsproblems durch eine Integralgleichung. *Zeitschrift für Physik*, 126(7-9):609–618, 1949.

[21] Ma. Messner, Mi. Messner, F. Rammerstorfer, and P. Urthaler. Hyperbolic and Elliptic Numerical Analysis BEM library. http://www.mech.tugraz.at/HyENA, 2010.

[22] J. Nedelec. Integral equations with nonintegrable kernels. *Integral Equations and Operator Theory*, 5:563–672, 1982.

[23] N. Nishimura and S. Kobayashi. A regularized boundary intgral equation method for elastodynamic crack problems. *Computational Mechanics*, 4:319–328, 1989.

[24] M. Schanz. *Wave Propagation in Viscoelastic and Poroelastic Continua*, volume 2 of *Lecture Notes in Applied Mechanics*. Springer, 2001.

[25] M. Schanz. Poroelastodynamics: Linear Models, Analytical Solutions, and Numerical Methods. *Applied Mechanics Review*, 62(3):030803–1–030803–15, 2009.

[26] M. Schanz. On a reformulated convolution quadrature based boundary element method. *Computer Modelling in Engineering and Sciences*, 58(2):227–249, 2010.

[27] M. Schanz and A. H. D. Cheng. Transient wave propagation in a one-dimensional poroelastic column. *Acta Mechanica*, 145:1–18, 2000.

[28] O. Steinbach. *Numerical Approximation Methods for Elliptic Boundary Value Problems*. Springer, 2008.

[29] Th. Wiebe and H. Antes. A time domain integral formulation fo dynamic poroelasticity. *Acta Mechanica*, 90:125–137, 1991.